Final version of this article published as: David F. Ester & Vance E. Williams (2019) Exploiting molecular symmetry reduction to enrich liquid crystal phase diversity, *Liquid Crystals*, DOI: 10.1080/02678292.2019.1575991
https://doi.org/10.1080/02678292.2019.1575991

Exploiting Molecular Symmetry Reduction to Enrich Liquid Crystal Phase Diversity

*David F. Ester,[a] and Vance E. Williams[a]**

Department of Chemistry, Simon Fraser University, Burnaby, BC V5A 1S6 Canada.

Fax: 778-782-3765; Tel: 778-782-8059; E-mail: vancew@sfu.ca

The strategic tuning of liquid crystalline phase behaviour by adjusting molecular symmetry was investigated. A family of sixteen symmetrical and unsymmetrical 2,6-di(4'-n-alkoxybenzoyloxy) naphthalene derivatives were prepared and their liquid crystal properties examined by differential scanning calorimetry, polarised optical microscopy, and x-ray diffraction. All mesogens formed nematic phases, with longer-chain analogues also exhibiting smectic C phases at lower temperatures. Melting temperatures of the compounds strongly depend on molecular symmetry, whereas clearing transitions are relatively insensitive to this effect. A detailed analysis indicates that the clearing point can be predicted based on the nature of the terminal alkyl chains, with only a secondary effect from molecular symmetry. Moreover, low symmetry molecules showed a greater tendency to form smectic C phases, which was ascribed to the selective depression of the melting point versus the SmC-N transition. This demonstrates that molecular symmetry-breaking is a valuable tool both for tuning liquid crystalline phase range and for increasing a material's polymorphism.

Keywords: phase transitions, liquid crystals, nematic, smectic, molecular symmetry, polymorphism, structure-property relationships, self-assembly

1. Introduction

Liquid crystalline (LC) materials' unique combination of physical, optical, and electronic properties have led to their widespread use in myriad applications, including display devices,[1–4] biomedical imaging,[5–7] drug delivery,[8–12] thermography,[13–15] lasing,[16–18] and organic semiconductors.[19–23] The suitability of a liquid crystal for a given function depends both on the type of phase (e.g.

nematic, smectic, columnar, etc.) and the temperature range over which it is stable. Because self-assembly processes are highly sensitive to molecular structure, designing materials that exhibit both the desired LC properties and the physical, optical and electronic characteristics required for the target application remains an important but difficult challenge. In this context, we have demonstrated that molecular symmetry provides a useful handle for controlling the phase behavior of liquid crystalline materials, as symmetry-breaking tends to depress the solid-to-LC melting transition (T_m) without substantially altering either the clearing (T_c) or LC-LC transition temperatures, resulting in broader mesophases.[24–28]

In the present work, we explore whether the selective destabilisation of the melting point can be exploited to uncover "hidden" LC phases. Consider a hypothetical liquid crystal with a T_c that lies below the melting point of the solid phase; the LC would either not be observed, or would form only a metastable monotropic phase on cooling (Figure 1a, top). Using symmetry-breaking to depress the melting point below the clearing point could thus give rise to an enantiotropic liquid crystal phase (Figure 1a, bottom) observed on both heating and cooling. Because LC-LC transitions also appear to be relatively insensitive to symmetry effects, this approach could be used to unmask additional phases in cases where the symmetric analog exhibits one or more mesophases (Figure 1b). As such, lowering the molecular symmetry could serve not only to broaden existing phases, but to enrich the phase diversity.

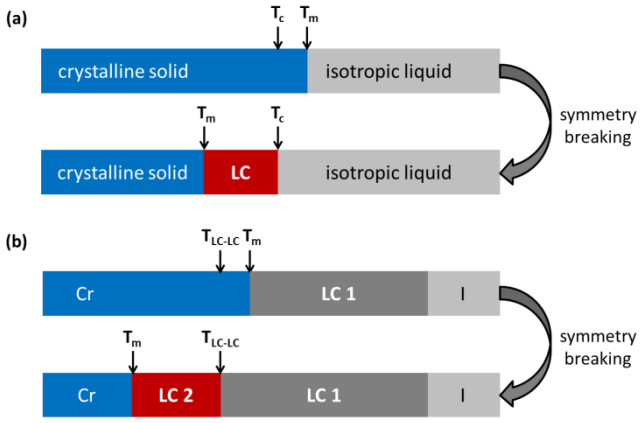

Figure 1. The potential effects of symmetry breaking on the phase behaviour of a material without (a) or with (b) an existing LC phase. Cr = crystalline solid, I = isotropic liquid.

To test this idea, we prepared a family of 2,6-di(4'-n-alkoxybenzoyloxy)naphthalenes **NP(m,n)** (Figure 2), symmetric derivatives of which (*i.e.* m=n) have been reported to possess nematic (N) phases over broad temperature ranges.[29–33] Notably, the highest reported homologue in this series, **NP(10,10)**, also exhibits a smectic C (SmC) mesophase below its nematic phase.[31] We speculated that other members of this series might also assemble into SmC phases if the melting temperature could be sufficiently depressed via symmetry breaking. Compounds that exhibit SmC-N transitions are relatively uncommon,[34–38] yet are attractive targets that could potentially avoid buckling defects associated with layer-contraction of SmC LCs cooled from SmA phases, which are known to degrade the performance of ferroelectric liquid crystals.[39–43]

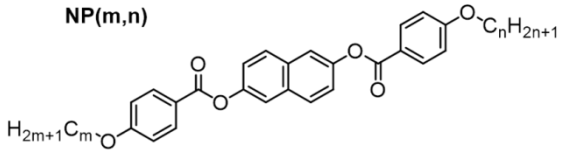

	m + n	symmetric	unsymmetric		
		NP(4,4)			
series 1	10	**NP(5,5)**	**NP(6,4)**		
series 2	12	**NP(6,6)**	**NP(7,5)**	**NP(8,4)**	
series 3	14	**NP(7,7)**	**NP(8,6)**	**NP(9,5)**	**NP(10,4)**
series 4	16	**NP(8,8)**	**NP(9,7)**	**NP(10,6)**	
series 5	18	**NP(9,9)**	**NP(10,8)**		
		NP(10,10)			

Figure 2. Compounds prepared for this study.

Nine unsymmetrical (m≠n) **NP(m,n)** derivatives with chains ranging from four to ten carbons in length (Figure 2) were synthesised in order to evaluate the effects of symmetry-breaking. The seven symmetric derivatives (m=n=4-10) previously reported in the literature were also prepared in order to confirm their phase assignments and to enable direct comparisons to the newly prepared low-symmetry analogues. In our initial analysis, the properties of derivatives with two chains of unequal lengths (m≠n) were compared to those of their symmetric isomers. To facilitate this discussion, fourteen of the derivatives were arranged into five isomeric series. The two remaining symmetric compounds, **NP(4,4)** and **NP(10,10)**, are included in order to examine the group additivity effects in systems that contain either butyl or decyl chains, respectively (*vide infra*).

2. Results and Discussion

2.1: Synthesis

Symmetric **NP(m,n)** derivatives were synthesised by the reaction of 2,6-dihydroxynaphthalene with two equivalents of the corresponding 4-alkoxybenzoic acid,

employing conditions similar to those described by Tsakos *et al.*[44] (Scheme 1, *route a*). This route was initially used to prepare **NP(7,7)** and **NP(9,9)** in yields of 37% and 68%, respectively, after purification. The remaining symmetric derivatives were isolated as side products during the synthesis of unsymmetrical derivatives outlined below.

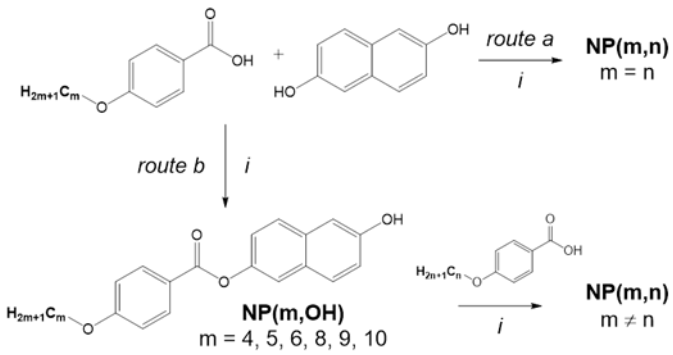

Scheme 1. Synthesis of diester **NP(m,n)** compounds studied. Conditions: i) 1) DMAP and 2) EDCI, CH_2Cl_2, reflux, 24h.

The unsymmetrical derivatives were prepared as illustrated in *route b* of Scheme 1. In the first step of this procedure, the appropriate 4-alkoxybenzoic acid was treated with an excess of 2,6-dihydroxynaphthalene to favor the production of the monoalkylated **NP(m, OH)** product. The **NP(m,m)** products with m = 4, 5, 6, 8, and 10 were also obtained as side products and isolated in 32-67% yields. After separation, the mono-substituted product was reacted with a second benzoic acid to afford the final **NP(m,n)** products in yields of 40-75%.

2.2: LC Characterisation

The liquid crystalline properties of all compounds were investigated by differential scanning calorimetry (DSC), polarised optical microscopy (POM), and variable temperature x-ray diffraction (VT-XRD), the results of which are summarised in Tables 1-6. The shorter chain-length symmetrical compounds (m = n = 4-7) exhibited

similar DSC and POM results. As a representative example, the DSC thermogram of **NP(5,5)** displays two peaks upon heating and three peaks on cooling; all peaks were observed on repeated heating/cooling cycles (Table 1). Upon cooling from the isotropic liquid, POM of this compound revealed the formation of a fluid phase that exhibits schlieren textures characteristic of a nematic phase (Figure 3a). Below the next transition at 118 °C, the texture rapidly transforms to a needle-like crystals with no observable fluidity (Figure 3b). The additional lower temperature peak observed in the DSC cooling curve does not correlate with any further changes by POM, and was attributed to a crystal-to-crystal transition. Similarly, **NP(4,4)**, **NP(6,6)**, and **NP(7,7)** were also found to exhibit crystalline – nematic – isotropic phase sequences. These results are in agreement with the existing literature for these symmetric **NP(m,n)** derivatives.[30–33]

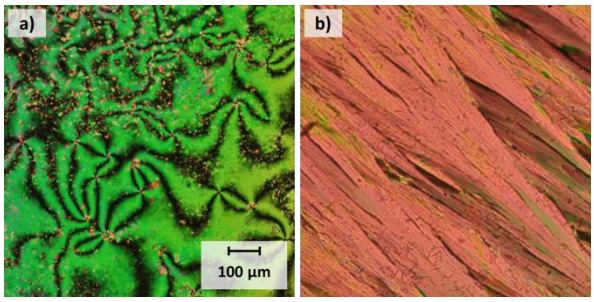

Figure 3. Polarised optical micrograph of **NP(5,5)** showing schlieren textures at 270 ˚C (a) and needle-like textures at 116 ˚C (b).

The longer chain symmetrical derivatives exhibit more complex mesophase behaviour, as demonstrated by the example of **NP(10,10)**. The DSC shows three peaks on heating and four peaks on cooling that are consistently observed on repeated heating/cooling cycles (Table 6). The XRD diffraction pattern of the phase just below the highest temperature transition (215 °C) (Figure 4a) consists of two low intensity broad peaks, indicating a lack of positional order, which is typical of a nematic phase. A nearly identical XRD pattern is observed upon cooling to just above the next phase

transition (176 °C) (Figure S4), verifying that this structure is maintained over the entire phase range. Below the next transition (161 °C) (Figure 4b), a sharp peak indexed to d_{001} develops in the low angle region, consistent with the onset of lamellar ordering. The corresponding layer spacing of 30.3 Å is considerably shorter than the molecular length of 47.4 Å calculated by molecular modelling, which suggests that the molecules adopt a tilted orientation within each layer. Combined with the broad peak observed in the high angle region, indicative of a lack of positional order within individual layers, this XRD pattern points to the formation of a SmC phase. At room temperature (Figure 4c), the low angle d_{001} peak disappears, suggesting the loss of lamellar order, and numerous sharp high angle peaks develop, indicating the formation of a crystalline solid.

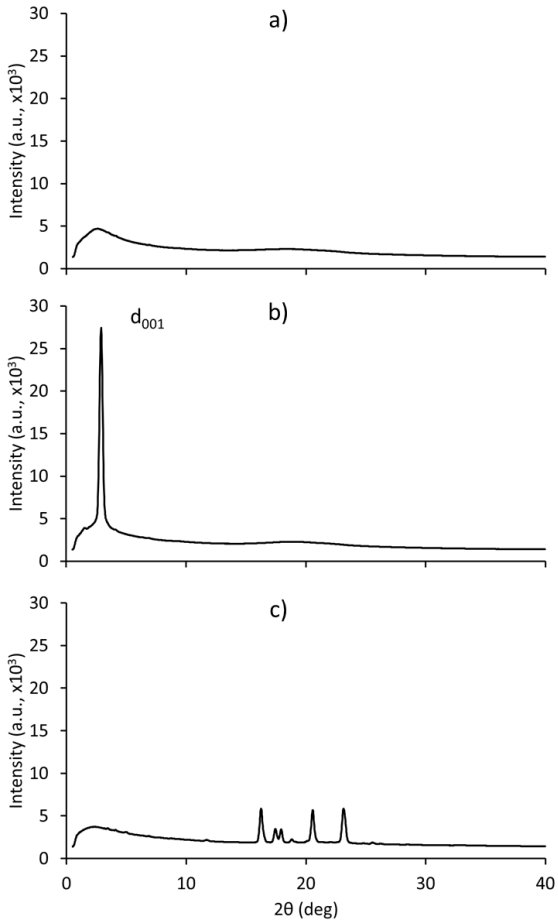

Figure 4. The XRD of **NP(10,10)** at 215 ˚C (a), 161 ˚C (b), and 25 °C (c).

The POM results provide further evidence for this phase sequence. The fluid schlieren textures (Figure 5a) of the high temperature nematic phase are once again formed. Cooling to below the subsequent phase transition at 170 °C, we observe the sudden onset of a fingerprint-like texture (Figure 5b), which quickly gives way to a modified schlieren texture of the SmC phase (Figure 5c). These intermediate "transition bars" are commonly observed features of N-SmC transitions.[45–51] At room temperature, needle-like crystallites (Figure S1) similar to those observed for **NP(5,5)** are formed. Thus, in keeping with the previous report[31], our DSC, POM, and XRD data confirm a sequence of crystalline – smectic C – nematic – isotropic phases for **NP(10,10)**.

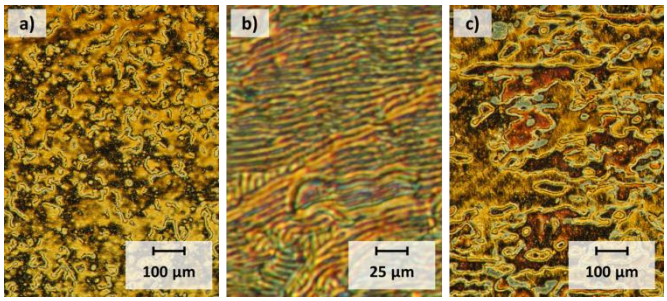

Figure 5. Polarised optical micrograph of **NP(10,10)** at 220 ˚C (a), 171 ˚C (b), and 168 ˚C (c).

Our findings for the symmetric **NP(8,8)** and **NP(9,9)** derivatives deviate from those of Pastorelli et al.[32], who, on the basis of POM studies, reported that these compounds exhibit only a nematic mesophase. Our observations confirm the formation of a nematic liquid crystal for both compounds, with melting and clearing points in good agreement with this earlier work. However the DSC thermogram of **NP(9,9)** shows an additional low enthalpy peak between the melting and clearing transitions, indicating the formation of an intermediate phase. This peak is observed on both heating and cooling, with limited hysteresis, suggesting an LC-LC transition. POM and XRD studies (see ESI) demonstrate that this is a SmC phase. While we observed phase

behavior for **NP(8,8)** on heating that is consistent with Pastorelli's findings, we note that this compound forms a previously unreported monotropic SmC on cooling.

Like their symmetric isomers, the unsymmetrical compounds in series 1 (m+n=10) and 2 (m+n=12) possess crystalline – nematic – isotropic phase sequences. Derivatives in series 3 (m+n=14) exhibit more complex polymorphism. **NP(10,4)**, consistent with its symmetric analog **NP(7,7)**, possesses only a nematic mesophase on heating and cooling. In contrast, **NP(8,6)** and **NP(9,5)** both form additional monotropic SmC phases on cooling. The unsymmetrical compounds in series 4 and 5, like **NP(9,9)** and **NP(10,10)**, display crystalline – SmC – nematic – isotropic phase sequences on heating and cooling; the SmC phases in these cases are all enantiotropic.

Table 1: Phase behaviour of series 1 (m+n = 10).

Compound	Phase[a]	T_t/°C (ΔH/kJ mol^{-1})[b] ⇌	Phase[a]	T_t/°C (ΔH/kJ mol^{-1})[b] ⇌	Phase[a]	T_t/°C (ΔH/kJ mol^{-1})[b] ⇌	Phase[a]
NP(5,5)	Cr 1	113.7 (-7.3)	Cr 2	147.5 (53) / 118.1 (-19)	N	273.4 (1.8) / 272.9 (-1.8)	I
NP(6,4)	Cr 1	101.1 (-18)	Cr 2	125.2 (21) / 106.8 (-1.1)	N	281.3 (2.0) / 280.5 (-2.0)	I

[a] as identified by POM and XRD, Cr = crystalline, Sm = smectic, N = nematic, I = isotropic, see discussion for details.
[b] transition temperatures and enthalpies determined by DSC at a scan rate = 10 °C/min.

Table 2: Phase behaviour of series 2 (m+n = 12).

Compound	Phase[a]	T_t/°C (ΔH/kJ mol^{-1})[b] ⇌	Phase[a]	T_t/°C (ΔH/kJ mol^{-1})[b] ⇌	Phase[a]	T_t/°C (ΔH/kJ mol^{-1})[b] ⇌	Phase[a]
NP(6,6)	Cr 1	127.3 (-8.9) / 116.2 (-29)	Cr 2	144.6 (34)	N	263.2 (2.2) / 262.7 (-1.8)	I
NP(7,5)	Cr 1	101.6 (-2.1)	Cr 2	122.5 (21) / 104.7 (-16)	N	256.9 (1.5) / 256.6 (-1.5)	I
NP(8,4)			Cr	117.5 (27) / 99.0 (-22)	N	264.3 (2.3) / 263.7 (-2.4)	I

[a] as identified by POM and XRD, Cr = crystalline, Sm = smectic, N = nematic, I = isotropic, see discussion for details.
[b] transition temperatures and enthalpies determined by DSC at a scan rate = 10 °C/min.

Table 3: Phase behaviour of series 3 (m+n = 14).

Compound	Phase[a]	T_t /°C (ΔH/kJ mol^{-1})[b]	Phase[a]	T_t /°C (ΔH/kJ mol^{-1})[b]	Phase[a]	T_t /°C (ΔH/kJ mol^{-1})[b]	Phase[a]
NP(7,7)			Cr	153.1 (37) 122.8 (-39)	N	244.9 (1.5) 244.1 (-1.3)	I
NP(8,6)	Cr	107.8 (-29)	Sm C	127.0 (32) 114.9 (-1.4)	N	249.6 (1.6) 248.7 (-1.6)	I
NP(9,5)	Cr	97.9 (-18)	Sm C	117.6 (37) 109.2 (-1.2)	N	247.2 (1.6) 246.6 (-1.6)	I
NP(10,4)			Cr	114.7 (25) 102.8 (-23)	N	250.7 (1.6) 250.4 (-1.7)	I

[a] as identified by POM and XRD, Cr = crystalline, Sm = smectic, N = nematic, I = isotropic, see discussion for details.
[b] transition temperatures and enthalpies determined by DSC at a scan rate = 10 °C/min.

Table 4: Phase behaviour of series 4 (m+n = 16).

Compound	Phase[a]	T_t /°C (ΔH/kJ mol^{-1})[b]	Phase[a]	T_t /°C (ΔH/kJ mol^{-1})[b]	Phase[a]	T_t /°C (ΔH/kJ mol^{-1})[b]	Phase[a]
NP(8,8)	Cr	126.5 (-32)	Sm C	144.5 (35) 142.3 (-1.6)	N	238.4 (1.5) 237.9 (-1.4)	I
NP(9,7)	Cr	129.5 (38) 105.7 (-35)	Sm C	142.0 (2.0) 140.8 (-1.8)	N	235.7 (1.7) 235.1 (-1.8)	I
NP(10,6)	Cr	116.9 (33) 94.2 (-30)	Sm C	129.8 (1.2) 129.0 (-1.2)	N	233.2 (1.6) 232.3 (-1.5)	I

[a] as identified by POM and XRD, Cr = crystalline, Sm = smectic, N = nematic, I = isotropic, see discussion for details.
[b] transition temperatures and enthalpies determined by DSC at a scan rate = 10 °C/min.

Table 5: Phase behaviour of series 5 (m+n = 18).

Compound	Phase[a]	T_t /°C (ΔH/kJ mol^{-1})[b]	Phase[a]	T_t /°C (ΔH/kJ mol^{-1})[b]	Phase[a]	T_t /°C (ΔH/kJ mol^{-1})[b]	Phase[a]
NP(9,9)	Cr	144.0 (42) 120.9 (-42)	Sm C	160.6 (1.5) 160.3 (-1.9)	N	228.7 (1.3) 228.4 (-1.2)	I
NP(10,8)	Cr	124.3 (35) 104.3 (-34)	Sm C	157.1 (2.0) 156.7 (-2.1)	N	228.5 (1.6) 228.1 (-1.5)	I

[a] as identified by POM and XRD, Cr = crystalline, Sm = smectic, N = nematic, I = isotropic, see discussion for details.
[b] transition temperatures and enthalpies determined by DSC at a scan rate = 10 °C/min.

Table 6: Phase behaviour of **NP(4,4)** and **NP(10,10)**.

Compound	Phase[a]	T_t /°C (ΔH/kJ mol^{-1})[b]	Phase[a]	T_t /°C (ΔH/kJ mol^{-1})[b]	Phase[a]	T_t /°C (ΔH/kJ mol^{-1})[b]	Phase[a]	T_t /°C (ΔH/kJ mol^{-1})[b]	Phase[a]
NP(4,4)	Cr 1	109.9 (-10)	Cr 2	139.1 (-1.8)	Cr 3	160.7 (30) 142.3 (-15)	N	302.4 (2.3) 301.7 (-2.1)	I
NP(10,10)	Cr 1	111.7 (-4.5)	Cr 2	135.3 (40) 113.5 (-30)	Sm C	170.8 (2.4) 170.6 (-2.5)	N	221.5 (1.5) 221.2 (-1.5)	I

[a] as identified by POM and XRD, Cr = crystalline, Sm = smectic, N = nematic, I = isotropic, see discussion for details.
[b] transition temperatures and enthalpies determined by DSC at a scan rate = 10 °C/min.

2.3: Symmetry Effects

Having determined the phase behaviour of these compounds, we turned our attention to the impact of molecular symmetry on the LC phase ranges. In order to provide an overview of all sixteen **NP(m,n)** compounds, their phase behaviour is presented graphically in Figure 6, with compounds sorted into isomeric series 1-5.

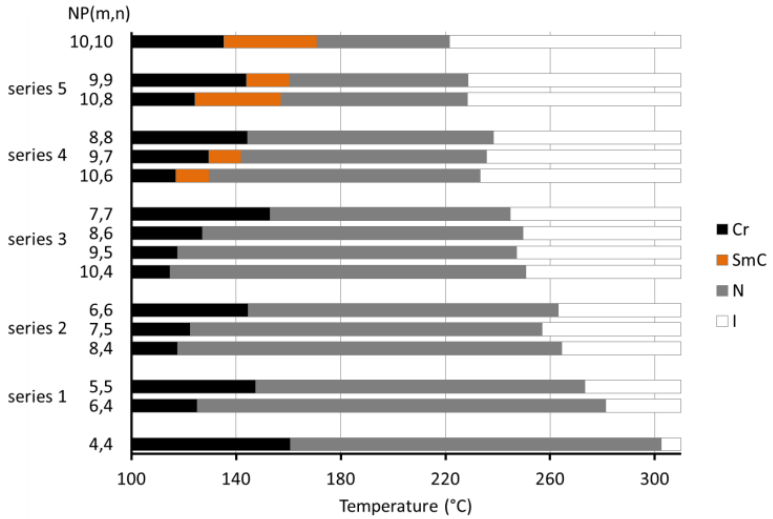

Figure 6. LC phase behaviour of the **NP(m,n)** compounds upon heating.

Our initial analysis followed an approach inspired by Thomas Carnelley's observation that unsymmetrical molecules melt at lower temperatures than their more symmetric isomers.[24–28,52,53] For this reason, we compared isomeric compounds with different degrees of symmetry. An examination of the phase behaviour within each isomer series reveals clear trends with respect to the melting point (T_m, black-grey/orange boundary). Without exception, low symmetry compounds melt at lower temperatures than the corresponding symmetric isomer, with an average depression of -25.9 °C. The magnitude of this melting depression increases as the disparity between *m* and *n* increases within a series. In contrast, the clearing point (T_c, grey-white boundary) exhibits small positive and negative fluctuations, with an average change of +0.8 °C, associated with symmetry-breaking. As a result of these conflicting effects, less symmetric isomers uniformly display expanded LC phase ranges, with an average

increase of 26.8 °C. These results are consistent with earlier studies on both columnar and highly ordered lamellar mesophases.[24–28] Collectively, these findings demonstrate that molecular shape and symmetry, in large part determined by the chain lengths on the periphery of a mesogen, is a major determinant of LC phase formation and stability as recently argued by Goodby.[54]

As noted above, the clearing temperatures of low symmetry **NP(m,n)** derivatives were in some cases higher than their more symmetrical isomers. The most pronounced example is **NP(6,4)**, which has a T_c that is almost 8 °C higher than that of **NP(5,5)**. These observations suggest that factors other than molecular symmetry may dominate; for example, if odd-even effects have a significant impact on T_c, then replacing two odd-numbered C-5 chains in **NP(5,5)** with even-numbered C-6 and C-4 chains in **NP(6,4)** could plausibly cause the observed elevation in T_c, irrespective of symmetry. More generally, while clearing temperatures of the symmetrical derivatives tend to decrease with increasing chain length (Figure 7), this variation is markedly nonlinear; similar trends have been noted across other mesogenic series.[55] This non-uniform trend indicates that the specific chain lengths, and not just the average number of carbons, should be considered in assessing symmetry effects.

With these consideration in mind, we undertook an alternative analysis based on a group additivity approach that assumes that the contribution of a chain should, in the absence of symmetry effects, be the same from molecule to molecule. A similar analysis was employed by Attard and coworkers in their examination of non-symmetric dimers.[56] Thus, the T_c of **NP(6,4)** could be usefully approximated by taking the average value of the two symmetric isomers **NP(6,6)** and **NP(4,4)**. Indeed, this group additivity approach predicts a clearing temperature of 282.8°C, in good agreement with the observed value of 281.3°C.

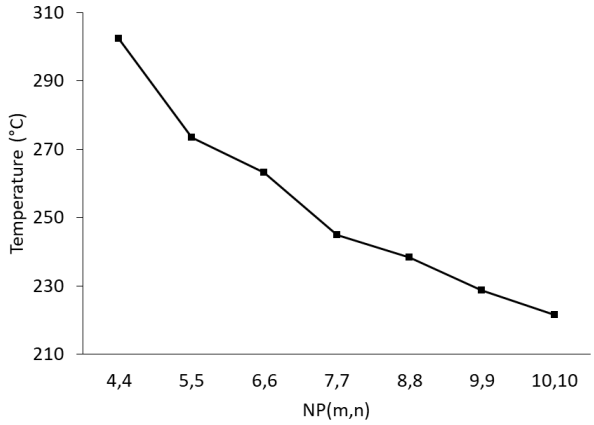

Figure 7. Clearing temperatures (T_c) of the symmetric **NP(m,n)** derivatives.

More generally, we compared the experimentally-determined T_c of unsymmetrical **NP(m,n)** derivatives to the temperatures predicted by this group additivity approach, *i.e.* the average T_c for the two symmetric analogs **NP(m,m)** and **NP(n,n)** (Figure 8a). The analogous comparison between the experimentally observed T_c and the values of the corresponding symmetric isomer are shown in Figure 8b. In both plots, the compounds are grouped according to chain length disparity, (m-n), since symmetry effects in T_m were noted to increase with m-n. For cases where the discrepancy in chain lengths is small (m-n=2), the trends in observed T_c closely parallel the predictions based on group additivity, with the predicted and observed values in all cases being within 1-2 °C. In contrast, the prediction based on symmetric isomers alternates between values that are too high or too low. Hence, it appears that the group additivity approach provides a more reliable estimate of clearing temperature than a simple comparison between isomers with distinct symmetries.

Figure 8b shows a marked odd-even effect for (m-n=2); unsymmetrical molecules with even-numbered carbon alkyl chains have higher than predicted clearing temperatures, whereas those with an odd number of carbons are lower than predicted. A subtle odd-even effect is also apparent in the plot of T_c of the symmetrical derivatives as

a function of chain length (Figure 7), and may underlie the trends in Figure 8b. Hence, when an unsymmetrical derivative with two even carbon chains, such as **NP(6,4)**, is compared to its symmetric isomer, **NP(5,5)**, the odd-even effect elevates the T_c of the former. Conversely, this model correctly predicts that **NP(5,7)** should clear at a lower temperature than its isomer **NP(6,6)**, regardless of symmetry considerations.

For m–n=4, both the symmetric and unsymmetrical isomers have chains with the same parity, so the odd-even effect should have a negligible impact. In this case, the group additivity predictions diverge from the observed T_c with the unsymmetrical compounds having uniformly lower clearing temperatures than predicted. This suggests that molecular symmetry does cause a depression of T_c, albeit the magnitude of the effect is significantly smaller than for T_m. This is in line with our earlier result for T_m; symmetry effects become more pronounced at greater chain length disparity. Therefore, our analysis indicates that there is a balance between odd-even and symmetry effects that govern the clearing temperature. At small chain length disparity (m-n=2) odd-even effects dominate, whereas at larger chain length differences (m-n=6) symmetry effects become significant.

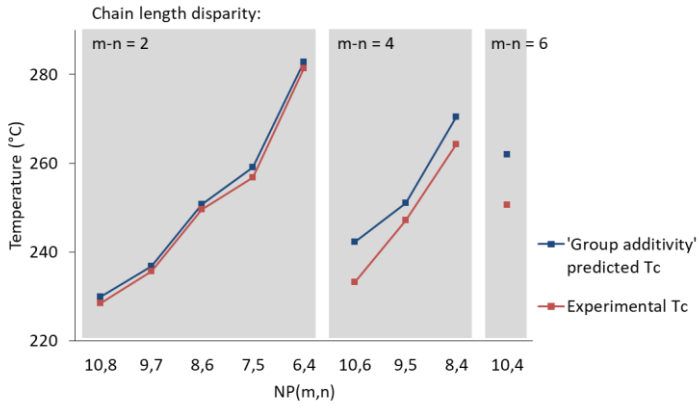

a)

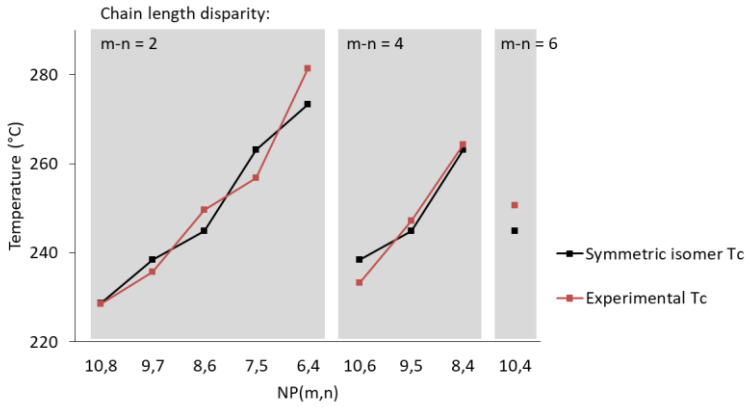

b)

Figure 8. Comparison of the experimental clearing points (T_c) for the unsymmetric compounds to the 'group additivity' predictions (a) and the respective symmetric isomer values (b). See discussion for details of predicted values.

When the group additivity approach was applied to the melting temperature, we found that the predicted T_m values differed significantly from those of the isomer comparison approach (Figure 9). However, both models predict melting points that are substantially higher than the experimentally-determined values, with an increased effect at larger chain length disparities. Thus, while neither model provides a reliable prediction of T_m, both support the conclusion that symmetry-breaking serves to depress this transition.

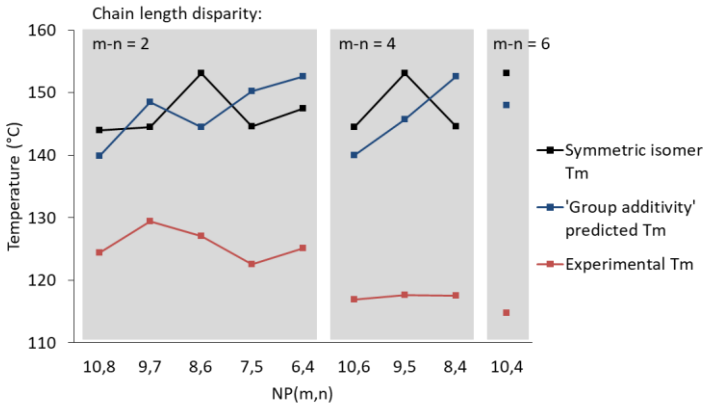

Figure 9. Comparison of the experimental melting points (T_m) for the unsymmetric compounds to the respective symmetric isomer values and the 'group additivity' predictions. See discussion for details of predicted values.

What of the prediction, outlined in Figure 1, that selective suppression of T_m could lead to not just broader mesophases, but also increased phase diversity? Of the symmetric derivatives, only **NP(9,9)** and **NP(10,10)** form SmC phases on both heating and cooling. The unsymmetrical **NP(10,8)** also forms an enantiotropic smectic phase, with a SmC-N transition temperature (157.1°C) that is similar to that of **NP(9,9)**. However, because the former compound has a lower melting point, its smectic phase range (33°C) is considerably broader than that of the latter (17°C). Notably, because both the SmC-N transition and T_c are relatively insensitive to symmetry effects, these compounds exhibit similar nematic temperature ranges.

The shorter-chain symmetrical derivatives show a decreased tendency to form smectic phases. Thus, **NP(8,8)** exhibits a monotropic SmC phase, only observed upon cooling. However, its low symmetry isomers, **NP(10,6)** and **NP(9,7)** both possess enantiotropic SmC phases over ranges of 12-13° C. This difference can be understood in terms of the selective depression of T_m by symmetry-breaking. The monotropic nematic-SmC transition of **NP(8,8)** lies approximately 2° C below the melting point; the smectic phase is observed only because of hysteresis between the freezing and melting points. Whereas **NP(9,7)** has a similar SmC-N transition temperature as **NP(8,8)**,

desymmetrisation lowers the melting point of the former by approximately 15°C, allowing the smectic phase to persist on heating as well as on cooling.

The symmetric homologs with even shorter chain lengths fail to exhibit SmC phases on either heating or cooling, presumably because the melting points lie well above the SmC-N transition temperatures. However, while **NP(7,7)** lacks a smectic phase, two of its isomers, **NP(8,6)** and **NP(9,5)**, form monotropic SmC phases upon cooling. The remaining isomer in this series, **NP(10,4)**, exhibits only a nematic mesophase. No smectic phases were observed for either **NP(6,6)**, **NP(5,5)** or any of their isomers. These results highlight a key constraint of the approach presented in Figure 1: while it is indeed possible to uncover "hidden" SmC phases through symmetry breaking, this strategy is limited by the extent to which T_m can be lowered and the relative position of the SmC-N transition. In the present system, the suppression of T_m appears to be insufficient to overcome the dramatic reduction of the SmC-N transition at shorter chain lengths. Nevertheless, we have successfully demonstrated expanded phase ranges, new enantiotropic phases, or exposed monotropic phases of the SmC phase in the low symmetry isomers of **NP(9,9)**, **NP(8,8)** and **NP(7,7)**.

3. Conclusions

In the present work, we have examined the impact of molecular symmetry as a means to broaden liquid crystal temperature ranges and to increase the number of thermodynamically stable mesophases. The sixteen symmetrical, NP(n,n) and unsymmetrical, NP(m,n), naphthalene mesogens examined all form nematic mesophases, with low symmetry analogs exhibiting an increased tendency to form SmC phases. This represents a potentially useful strategy for the creation of materials with specified phase sequences. Moreover, our results demonstrate that phase sequences seen

only at high molecular weights within a symmetrical series can be observed for smaller low-symmetry analogs, which opens the door to the design of liquid crystals that are compatible with vapour deposition methods. Such materials could also be more easily solution processed because both lower molecular weights and decreased symmetry are known to increase solubility.[55–57]

Experimental Section

Materials and Methods

All solvents used were reagent grade. Methyl 4-hydroxy benzoate, 2,6-dihydroxynaphthalene, 4-dimethylamino pyridine (DMAP), and N-(3-dimethylaminopropyl)-N'-ethylenecarbodiimide hydrochloride (EDCI) were purchased from TCI America. All other reagents were purchased from Sigma-Aldrich. All reagents were used as received without further purification. 4-Alkoxybenzoic acids were prepared from methyl 4-hydroxybenzoate via alkylation followed by hydrolysis according to previously reported procedures.[60] Column chromatography was performed on silica gel 60 (230-400 mesh) purchased from Silicyle Inc. $CDCl_3$ was obtained from Cambridge Isotope Laboratories Inc.

400 MHz and 500 MHz ^{1}H NMR spectra were obtained on a Bruker AMX-400 400 MHz and Varian AS500 Unity Inova 500 MHz spectrometers, respectively. High resolution mass spectrometry was carried out on an Agilent 6210 TOF LC/MS (ESI+) by Hongwen Chen (SFU), and on a Bruker micrOTOF II LC/MS (ESI^+) by Nonka Sevova at Notre Dame Mass Spectrometry and Proteomics facility. Phase transition temperatures and enthalpies were determined using differential scanning calorimetry (DSC) on a TA Instruments DSC Q2000 equipped with a TA Instruments Refrigerated

Cooling System 90, heating and cooling at a rate of 10˚C min^{-1}. Polarised optical microscopy was carried out using an Olympus BX50 microscope equipped with a Linkam LTS350 heating stage. X-ray scattering experiments were conducted using a Rigaku R-Axis Rapid diffractometer equipped with an in-house built temperature controller.[61] Calculations were carried out by density functional theory (DFT) using B3LYP/3-21G* in Gaussian 09, details of which are provided in ESI.[58]

Synthesis

Symmetric derivatives NP(m,n) (m=n). In a flame-dried 50 ml round bottom flask, 2,6-dihydroxynaphthalene (0.2 g, 1.25 mmol) was dissolved in dry DCM (30 mL) under N_2. 4-alkoxybenzoic acid (2.75 mmol) was added followed by DMAP (3.75 mmol). This mixture was stirred at ~0 °C under N_2 for 15 minutes. EDCI (2.50 mmol) was then added and the mixture was stirred at ~0 °C under N_2 for 15 minutes before refluxing for 48 hours. The solution was then cooled to room temperature, and poured over ice; the organic phase was separated and washed with water (2 x 30 mL), 10% HCl (40 mL), and brine (40 mL). The organic phase was dried over $MgSO_4$ and the solvent was removed by rotary evaporation. This crude product was then purified by column chromatography on silica with dichloromethane as eluent. The solvent was removed under reduced pressure and the resulting product was recrystallised from ethyl acetate to afford a white solid in yields of 37-68 %. Note that several of the symmetric **NP(m,n)** compounds were isolated as side products of the monoester synthesis described below. Analytical data of the **NP(m,n)** (m=n) compounds can be found in the ESI.

Monoesters NP(m,OH). In a flame-dried 250 ml round bottom flask, 2,6-dihydroxynaphthalene (1.0 g, 6.24 mmol) was dissolved in dry DCM (100 mL) under N_2. The appropriate 4-alkoxybenzoic acid (4.16 mmol) was added, followed by DMAP

(6.66 mmol). This mixture was stirred at ~0 °C under N_2 for 15 minutes, at which time EDCI (4.16 mmol) was then added. This mixture was stirred at ~0 °C under N_2 for 15 minutes, then refluxed for 12 hours. The solution was then cooled to room temperature and the solid precipitate was removed by filtration. The solution was then poured over ice and the organic phase was separated and washed with water (2 x 100 mL), 10% HCl (100 mL), and brine (100 mL), then dried over $MgSO_4$ and the solvent was removed by rotary evaporation. This crude product was then purified by column chromatography on silica with a gradient from 5% to 40% of DCM in hexanes as the eluent. The first fraction was recrystallised from ethyl acetate to yield **NP(m,n)** (m=n) product as a white solid (32-67%). The second fraction was recrystallised from acetonitrile to yield **NP(m,OH)** product as a white solid (13-57%). Analytical data for the **NP(m,OH)** compounds can be found in the ESI.

Unsymmetrical derivatives NP(m,n) ($m \neq n$). In a flame-dried 50 ml round bottom flask, **NP(m,OH)** (0.1 g) was dissolved in dry DCM (25 mL) under N_2. The appropriate 4-alkoxybenzoic acid (1.5 equiv.) was added followed by DMAP (3 equiv.). This mixture was stirred at 0 °C under N_2 for 15 minutes. EDCI (2 equiv.) was then added. This mixture was stirred at 0 °C under N_2 for 15 minutes before refluxing for 48 hours. The solution was then cooled to room temperature, then poured over ice. The organic phase was separated and washed with water (2 x 25 mL), 10% HCl (30 mL), and brine (30 mL), then dried over $MgSO_4$ and the solvent was removed by rotary evaporation. The crude product was then purified by column chromatography on silica gel with dichloromethane as eluent. The resulting product was recrystallised from ethyl acetate to afford a white solid in yields of 40-75 %. Analytical data of the **NP(m,n)** ($m \neq n$) compounds can be found in the ESI.

Acknowledgements

We gratefully acknowledge the Natural Sciences and Engineering Research Council of Canada (NSERC) and Simon Fraser University (SFU) for funding. This work made use of the 4D Labs shared facilities supported by the Canada Foundation for Innovation (CFI), British Columbia Knowledge Development Fund (BCKDF), Western Economic Diversification (WD), and SFU.

Notes and References

[1] Wang Y-J, Chen P-J, Liang X, et al. Augmented reality with image registration, vision correction and sunlight readability via liquid crystal devices. Sci. Rep. 2017;7:433.

[2] Tokunaga S, Itoh Y, Yaguchi Y, et al. Electrophoretic Deposition for Cholesteric Liquid-Crystalline Devices with Memory and Modulation of Reflection Colors. Adv. Mater. 2016;28:4077–4083.

[3] Chapran M, Angioni E, Findlay NJ, et al. An Ambipolar BODIPY Derivative for a White Exciplex OLED and Cholesteric Liquid Crystal Laser toward Multifunctional Devices. ACS Appl. Mater. Interfaces. 2017;9:4750–4757.

[4] Mandle RJ, Cowling SJ, Goodby JW. Evaluation of 4-alkoxy-4′-nitrobiphenyl liquid crystals for use in next generation scattering LCDs. RSC Adv. 2017;7:40480–40485.

[5] Nakayama M, Kajiyama S, Kumamoto A, et al. Stimuli-responsive hydroxyapatite liquid crystal with macroscopically controllable ordering and magneto-optical functions. Nat. Commun. 2018;9:568.

[6] Kim HJ, Rim J, Jang C-H. Diagnosis of tuberculosis using a liquid crystal-based optical sensor. Macromol. Res. 2016;24:123–130.

[7] Miceli V, Meli V, Blanchard-Desce M, et al. In vitro imaging of β-cells using fluorescent cubic bicontinuous liquid crystalline nanoparticles. RSC Adv. 2016;6:62119–62127.

[8] Deng Y, Ling J, Li M-H. Physical stimuli-responsive liposomes and polymersomes as drug delivery vehicles based on phase transitions in the membrane. Nanoscale. 2018;10:6781–6800.

[9] Oyafuso MH, Carvalho FC, Takeshita TM, et al. Development and In Vitro Evaluation of Lyotropic Liquid Crystals for the Controlled Release of Dexamethasone. Polymers. 2017;9:330.

[10] Thapa RK, Choi JY, Poudel BK, et al. Multilayer-Coated Liquid Crystalline Nanoparticles for Effective Sorafenib Delivery to Hepatocellular Carcinoma. ACS Appl. Mater. Interfaces. 2015;7:20360–20368.

[11] Tran N, Hawley AM, Zhai J, et al. High-Throughput Screening of Saturated Fatty Acid Influence on Nanostructure of Lyotropic Liquid Crystalline Lipid Nanoparticles. Langmuir. 2016;32:4509–4520.

[12] Evenbratt H, Ström A. Phase behavior, rheology, and release from liquid crystalline phases containing combinations of glycerol monooleate, glyceryl monooleyl ether, propylene glycol, and water. RSC Adv. 2017;7:32966–32973.

[13] Zhang L, Wang L, Hiremath US, et al. Dynamic Orthogonal Switching of a Thermoresponsive Self-Organized Helical Superstructure. Adv. Mater. 2017;29:1700676.

[14] Tan Q, Liao J, Chen S, et al. Mesogen-jacketed liquid crystalline polymers with peripheral oligo(ethylene oxide) chains: phase structure and thermoresponsive behavior. Polym. Chem. 2014;5:5147–5159.

[15] Kakiuchida H, Ogiwara A. Reverse-mode thermoresponsive light attenuators produced by optical anisotropic composites of nematic liquid crystals and reactive mesogens. Opt. Mater. 2018;78:273–278.

[16] Coles H, Morris S. Liquid-crystal lasers. Nat. Photonics. 2010;4:676–685.

[17] Huang J-C, Hsiao Y-C, Lin Y-T, et al. Electrically switchable organo–inorganic hybrid for a white-light laser source. Sci. Rep. 2016;6:28363.

[18] Chapran M, Angioni E, Findlay NJ, et al. An Ambipolar BODIPY Derivative for a White Exciplex OLED and Cholesteric Liquid Crystal Laser toward Multifunctional Devices. ACS Appl. Mater. Interfaces. 2017;9:4750–4757.

[19] Iino H, Usui T, Hanna J. Liquid crystals for organic thin-film transistors. Nat. Commun. 2015;6:6828.

[20] Song M, Seo J, Kim H, et al. Ultrasensitive Multi-Functional Flexible Sensors Based on Organic Field-Effect Transistors with Polymer-Dispersed Liquid Crystal Sensing Layers. Sci. Rep. 2017;7:2630.

[21] Keum C-M, Liu S, Al-Shadeedi A, et al. Tuning charge carrier transport and optical birefringence in liquid-crystalline thin films: A new design space for organic light-emitting diodes. Sci. Rep. 2018;8:699.

[22] Kwak D, Choi HH, Kang B, et al. Tailoring Morphology and Structure of Inkjet-Printed Liquid-Crystalline Semiconductor/Insulating Polymer Blends for High-Stability Organic Transistors. Adv. Funct. Mater. 2016;26:3003–3011.

[23] He Y, Sezen M, Zhang D, et al. High Performance OTFTs Fabricated Using a Calamitic Liquid Crystalline Material of 2-(4-Dodecyl phenyl)[1]benzothieno[3,2-b][1]benzothiophene. Adv. Electron. Mater. 2016;2:1600179.

[24] Ester DF, Williams VE. Molecular symmetry effects on the stability of highly ordered smectic phases. Liquid Crystals. 2018; DOI: 10.1080/02678292.2018.1471746.

[25] Voisin E, Williams VE. The impact of molecular symmetry and shape on the stability of discotic liquid crystals. Can. J. Chem. 2017;96:132–138.

[26] Voisin E, Williams VE. Side-chain shuffling: regioselective synthesis of mixed tail discotic mesogens. RSC Adv. 2016;6:11262–11265.

[27] Voisin E, Johan Foster E, Rakotomalala M, et al. Effects of Symmetry on the Stability of Columnar Liquid Crystals. Chem. Mater. 2009;21:3251–3261.

[28] Foster EJ, Babuin J, Nguyen N, et al. Synthesis of unsymmetrical dibenzoquinoxaline discotic mesogens. Chem. Commun. 2004;18:2052–2053.

[29] Srinivasa HT, Palakshamurthy BS, Devarajegowda HC, et al. Synthesis, characterization, crystal structure and liquid crystal studies of some symmetric naphthalene derivative molecules. J. Mol. Struct. 2018;1173:620–626.

[30] Karamysheva LA, Koyshev EI, Titov VV. Mesomorphism of 2,6-disubstituted naphthalenes. Russian Journal of Organic Chemistry. 1976;12:2628–2629.

[31] Gonzalez Y, Ros MB, Serrano JL. Naphthalene System as Origin of Unconventionally Shaped Ferroelectric Liquid Crystals. Chem. Mater. 1994;6:1516–1525.

[32] Pastorelli L, Chiavari G, Arcelli A. Synthesis and characteristics of naphthalene derivatives: a study of the liquid crystal mesomorphic range. Annali di Chimica. 1973;63:195–199.

[33] Ober CK, Bluhm TL. Thermotropic liquid crystalline polyesters containing naphthalenic mesogenic groups. Polym. Bull. 1986;15:233–239.

[34] Stannarius R, Eremin A, Harth K. Stripe instabilities in menisci of free-standing smectic films with a direct transition from smectic C to an isotropic or nematic phase. Liq. Cryst. 2017;44:1201–1206.

[35] Kapernaum N, Wuckert E, Frey W, et al. Hunting for smectic C in calamitic azobenzene ionic liquid crystals with different cationic head groups. J. Phys. Org. Chem. [Internet]. 2018 [cited 2018 Apr 28];31. Available from: https://onlinelibrary.wiley.com/doi/abs/10.1002/poc.3779.

[36] Emelyanenko AV, Khokhlov AR. Simple theory of transitions between smectic, nematic, and isotropic phases. J. Chem. Phys. 2015;142:204905.

[37] Chołuj A, Kula P, Dąbrowski R, et al. Synthesis and mesomorphic properties of laterally fluorinated alkyl 4″-alkylterphenyl-4-yl carbonate liquid crystals. J. Mater. Chem. C. 2014;2:891–900.

[38] Walba DM, Korblova E, Huang C-C, et al. Reflection Symmetry Breaking in Achiral Rod-Shaped Smectic Liquid Crystals? J. Am. Chem. Soc. 2006;128:5318–5319.

[39] Zhang Y-S, Liu C-Y, Emelyanenko AV, et al. Synthesis of Predesigned Ferroelectric Liquid Crystals and Their Applications in Field-Sequential Color Displays. Adv. Funct. Mater. 2018;28:1706994.

[40] Knust S, Wahle M, Kitzerow H-S. Ferroelectric Liquid Crystals in Microcapillaries: Observation of Different Electro-optic Switching Mechanisms. J. Phys. Chem. B. 2017;121:5110–5115.

[41] Schubert CPJ, Müller C, Bogner A, et al. Design of liquid crystals with "de Vries-like" properties: structural variants of carbosilane-terminated 5-phenylpyrimidine mesogens. Soft Matter. 2017;13:3307–3313.

[42] Hird M. Designing Principles, Synthesis, and Properties of Smectic C Host Materials for Ferroelectric Liquid Crystals. Handb. Liq. Cryst. [Internet]. 2nd ed. Weinheim: Wiley-VCH Verlag GmbH & Co. KGaA; 2014. p. 237–261. Available from: https://onlinelibrary.wiley.com/doi/abs/10.1002/9783527671403.hlc132.

[43] Roberts JC, Kapernaum N, Song Q, et al. Design of Liquid Crystals with "de Vries-like" Properties: Frustration between SmA- and SmC-Promoting Elements. J. Am. Chem. Soc. 2010;132:364–370.

[44] Tsakos M, Schaffert ES, Clement LL, et al. Ester coupling reactions – an enduring challenge in the chemical synthesis of bioactive natural products. Nat. Prod. Rep. 2015;32:605–632.

[45] Gim M-J, Beller DA, Yoon DK. Morphogenesis of liquid crystal topological defects during the nematic-smectic A phase transition. Nat. Commun. [Internet]. 2017;8. Available from: https://www.ncbi.nlm.nih.gov/pmc/articles/PMC5459947/.

[46] Sparavigna A, Mello A, Massa G. Undulation textures at the phase transitions of some alkyloxybenzoic acids. Phase Transit. 2009;82:398–408.

[47] Dierking I. Ch. 7 - The Fluid Smectic Phases. Textures Liq. Cryst. Weinheim: Wiley-VCH Verlag GmbH & Co. KGaA; 2003. p. 91–122.

[48] Scheffer TJ, Gruler H, Meier G. Periodic free-surface disclination at nematic to smectic C phase transition. Solid State Commun. 1972;11:253–257.

[49] Kleman M. Defects in small-molecule and polymeric nematics. Liq. Cryst. 1989;5:399–417.

[50] Allet C, Kleman M, Vidal P. Striped patterns in a thin droplet of a smectic C phase. Journal de Physique. 1978;39:181–188.

[51] Kleman M. Microstructures of liquid crystals. Defects. Liq. Cryst. Plast. Cryst. 1974;1:76–91.

[52] Carnelley T. XXI. Chemical symmetry, or the influence of atomic arrangement on the physical properties of compounds. Lond. Edinb. Dublin Philos. Mag. J. Sci. 1882;13:180–193.

[53] Carnelley T. XIII. Chemical symmetry, or the influence of atomic arrangement on the physical properties of compounds. Lond. Edinb. Dublin Philos. Mag. J. Sci. 1882;13:112–130.

[54] Goodby JW. Free volume, molecular grains, self-organisation, and anisotropic entropy: machining materials. Liq. Cryst. 2017;44:1755–1763.

[55] Imrie CT, Taylor L. The preparation and properties of low molar mass liquid crystals possessing lateral alkyl chains. Liq. Cryst. 1989;6:1–10.

[56] Attard GS, Date RW, Imrie CT, et al. Non-symmetric dimeric liquid crystals The preparation and properties of the α-(4-cyanobiphenyl-4′-yloxy)-ω-(4-n-alkylanilinebenzylidene-4′-oxy)alkanes. Liq. Cryst. 1994;16:529–581.

[57] Ishikawa M, Hashimoto Y. Improvement in Aqueous Solubility in Small Molecule Drug Discovery Programs by Disruption of Molecular Planarity and Symmetry. J. Med. Chem. 2011;54:1539–1554.

[58] Pinal R. Effect of molecular symmetry on melting temperature and solubility. Org. Biomol. Chem. 2004;2:2692–2699.

[59] Lipinski CA. Drug-like properties and the causes of poor solubility and poor permeability. J. Pharmacol. Toxicol. Methods. 2000;44:235–249.

[60] Šepelj M, Lesac A, Baumeister U, et al. Dimeric Salicylaldimine-Based Mesogens with Flexible Spacers: Parity-Dependent Mesomorphism. Chem. Mater. 2006;18:2050–2058.

[61] Lavigueur C, Foster EJ, Williams VE. A simple and inexpensive capillary furnace for variable-temperature X-ray diffraction. J. Appl. Crystallogr. 2008;41:214–216.